Comparing C5Pe and Asphaltenes under Temperature and Pressure Reservoir Conditions using an Acoustic Wave Sensor

Marc Cassiède[*,†]*, Hervé Carrier*[†]*, Jean-Luc Daridon*[†]*, Sébastien Simon*[‡]*, and Johan Sjöblom*[‡]

[†]Universite de Pau et des Pays de l'Adour, E2S UPPA, CNRS, TOTAL, LFCR, UMR 5150, Pau, France

[‡]Ugelstad Laboratory, Department of Chemical Engineering, Norwegian University of Science and Technology (NTNU), N-7491 Trondheim, Norway

Corresponding author's email address : marc.cassiede@univ-pau.fr

KEYWORDS. Asphaltenes, Model compounds, Petroleum, Crude oil, Aggregation, Deposition, Viscosity, Quartz Crystal Resonator

ABSTRACT.

A quartz crystal resonator (QCR) was employed to assess the ability of C5Pe model asphaltene compound to form nanoaggregates in toluene and bigger flocs that adsorb on the QCR surfaces at higher concentration of flocculating agent. To allow comparison with real asphaltenes, experiments have been conducted in the same conditions on PetroPhase 2017 asphaltenes. First, the resonance properties of a QCR fully immersed in C5Pe/toluene solution were monitored during an isothermal titration experiment performed with *n*-heptane at atmospheric pressure.

Then, constant mass expansion experiments were carried out to evaluate whether C5Pe precipitate during isothermal depressurization of C5Pe/toluene + CH_4 systems with various CH_4 contents. The comparison between C5Pe and PetroPhase 2017 asphaltenes clearly revealed the propensity of C5Pe to self-associate in the presence of a flocculating agent whereas it shows a lower tendency than asphaltenes to deposit on gold surfaces.

1. INTRODUCTION

Crude oil production and transport pose intricate problems related to indigenous components in the crude oil and their interactions. These problems must be solved in order to guarantee a safe and regular production and transport. Major problems in the production chain concern deposition issues in the reservoir and on production facilities[1-3] together with separation of water and crude oil when oil is contacted with water.[4] W/O emulsions and the buildup of gel-like plugs with a high emulsified water content are issues of concern to disturb the flow pattern. All these phenomena can be traced back to the indigenous crude oil components able to stabilize emulsions. Hence it is of paramount importance to identify these species and to characterize them with regard to structure and chemistry. The major problem is that crude oils are a mixture of many different organic compounds and hence the identification of well-defined families is difficult. This hampers the discovery of clear structure-property relationships. A convenient way out of this dilemma is to synthesize organic molecules with a chemical structure averaging that of indigenous crude oil components and similar properties.[5] This strategy has for instance been successful to understand the interfacial,[6,7] self-association,[8-13] and flocculation[14] properties of asphaltenes. In this paper this concept has been further developed to study asphaltene precipitation and deposition under realistic production conditions.

The molecule investigated here is C5Pe which is an abbreviation of N-(1-hexylheptyl)-N'-(5-carboxylicpentyl)perylene-3,4,9,10-tetracarboxylic bisimide, which belongs to the perylene group introduced and studied by the group in Trondheim.[15] This molecule incorporates a fixed

hydrophobic moiety with a branched alkyl chain attached to a polyaromatic core (perylene) and with an acidic end group. In this way the molecule can mimic central interactions from the indigenous asphaltene molecules. These interactions are hydrogen bonding (due to the acidic group), pi-pi interactions (due to the aromatic core) and finally van der Waals interactions (due to the hydrocarbon chain).[16,17] All these interactions are central in crude oil media and can explain association and deposition phenomena of the asphaltene molecules[18,19] together with their interactions with other crude oil components. Although they present similarities in functionality, the differences in chemical structure between our single model compound and polydisperse natural asphaltenes can lead to differences in the extent of molecular aggregation in organic solvents.[20,21]

Asphaltenes in solution present complex properties with at least two self-association scales. First, asphaltenes self-associate to form nanometer-sized aggregates even in good solvents like toluene.[22] The size of these aggregates depends on the solvation state of asphaltenes as well as external parameters like temperature and pressure. Various models have been suggested to describe the structure of these aggregates.[23,24] Secondly, asphaltenes nanoaggregates destabilize to form aggregates of nanoaggregates (clusters) when the asphaltene solvation is reduced. This can happen when the pressure is reduced during oil production[25] and/or the oil is mixed with an incompatible fluid such as aliphatic solvent[26,27] or CO_2.[28] The flocculation kinetic is generally described by the diffusion-limited or reaction-limited cluster aggregation (DLCA or RLCA) models.[29]

Existing approaches used to sense the sizes of asphaltene aggregates in solution include optical microscopy,[30-32] light scattering[33] and UV-VIS spectroscopy[34]. In some cases the weak transmitted light through the sample can make the detection of asphaltenes challenging. As C5Pe model compound presents strong fluorescent intensity, C5Pe adsorption studies on polymer brush surfaces have been carried out by fluorescence microscopy.[35] However, the low

fluorescent intensity of natural asphaltenes prevents the correct determination of asphaltene adsorption amount by this technique. Therefore, alternative techniques which allow direct detection of asphaltene adsorption on inorganic surfaces are preferred. Among them, ellipsometry has been used to measure the thickness of asphaltenes films adsorbed on glass plates[36] and in another study, Wang et al.[20] characterized adsorption of C5Pe on mica surfaces in both toluene and heptane by a surface forces apparatus and obtained topographic images of the deposit by atomic force microscopy. Film thickness measurements were also performed in parallel on silicon wafers by ellipsometry. After comparing the results with those obtained on asphaltenes extracted from Athabasca bitumen (Alberta, Canada), they concluded that the asphaltenes and C5Pe model compound showed similar adsorption behavior to mica surfaces whereas much stronger aggregation of asphaltene molecules than C5Pe was observed, which was explained by the more complex nature of asphaltene molecules. Although these detection techniques are sensitive in the nanogramme range, they require that film thickness measurements are carried out at pre-defined times. To allow continuous monitoring of adsorption phenomena, other methods based on thickness shear mode resonators have been proposed.[37-41] These sensors are highly sensitive to their surrounding media and although their potential applications are difficult to extend to downhole measurements, they are in contrast very efficient in routine laboratory testing techniques to analyse the risk of asphaltene deposition and to evaluate the effectiveness of chemical inhibitors.[42] Therefore, quartz crystal resonators (QCR) have been extensively used[43-47] to study the deposition of asphaltenes destabilized in mixtures of aromatic solvents and light n-alkanes. These sensors have the potential to be used under high pressure conditions[28,41,48-51] and allow detecting the formation of the first asphaltene nanoaggregates with a size of 0.7 nm that form a monolayer on gold electrode surfaces.[48] The QCR device can be used to measure asphaltene aggregates formed in good solvent, with characteristic sizes of 3-10 nm[22] and bigger flocs of micrometer size which

are formed during the flocculation. However, the calculated amount of deposited asphaltene is sometimes larger than the actual value obtained from other techniques when the adsorbed film becomes viscoelastic.[52] For this reason further analysis of the resonance curves on several harmonics is necessary to measure the amount of asphaltenes deposited on gold surfaces using the QCR. In addition, as the damping of the shear wave generated by the quartz crystal depends on the viscosity and density of the contacting liquid, it is also sensitive to the phase changes occurring in binary systems composed of a crude oil and a gas. Among the potential applications, the QCR has been used to construct the phase diagram for different CO_2/crude oil system including the liquid-vapor phase transition and the asphaltene instability envelope.[28,48]

In order to determine the behavior of the model molecule under realistic *p* and *T* conditions we have undertaken atmospheric and high pressure QCR measurements. It consists in monitoring in real-time the changes in resonance properties of a quartz crystal sensor fully immersed in a C5Pe + toluene solution which has been destabilized with a flocculating agent. In the first part of this work that concerns ambient conditions, a continuous titration experiment with *n*-heptane of a C5Pe + toluene sample was performed and the *n*-heptane molar content at which C5Pe flocs start to appear was determined. In the second part the response of the quartz crystal sensor immersed in a C5Pe + toluene solution with various contents of injected CH_4 was studied during isothermal constant mass expansion (CME) experiments. These experiments were carried out using a high-pressure PVT cell with a quartz crystal shear mode resonator inside. The pronounced effects observed on the QCR response allowed to probe destabilization of either asphaltenes or C5Pe model molecules during a pressure scanning. This work also consists in comparing the results on C5Pe with real asphaltenes. For that purpose, PetroPhase 2017 asphaltenes (asphaltenes specially prepared for the 2017 PetroPhase conference) were chosen as they were thoroughly studied by several research groups,[53-59] and this way could

assess the ability of C5Pe to correctly represent the properties of asphaltene molecules under precipitation and deposition conditions.

2. EXPERIMENTAL SECTION

2.1. Chemicals and Materials. Samples of C5Pe molecules and PetroPhase 2017 asphaltenes were tested in this work. C5Pe was prepared according to the procedure by Nordgård et al.[6] PetroPhase 2017 asphaltenes were isolated from a Middle Eastern heavy crude oil, provided by Total, using standard ASTM D6560-12 method.[60] Toluene was used as the solvent of both compounds, whereas heptane was chosen as a titrant to generate flocculation. Both solvent and titrant were acquired from Fisher Sc. with a purity better than 99 % and were used without further purification. The CH_4 used in this work was purchased from Linde with a given purity better than 99.995 %.

2.2. Instrumental Setup. The two apparatus used for monitoring the resonance properties of the QCR at atmospheric pressure and under high pressure were already presented in previous works.[38,49,50]

2.2.1. Atmospheric pressure device. The apparatus mainly consists of a titration vessel and a flow titrant system. The titration cell, illustrated in Figure 1, is made up of a double wall glass cylinder. The interior cylinder presents two different diameters at the bottom and at the top. Titration is achieved from 0 to 90 % in a single run. A magnetic stirring bar rotating continuously into the sample allows stirring of the mixture. The vessel is closed by a cap with two electrical connections which are used to hold the QCR at the bottom of the cell. A heat-carrier fluid circulates between the two cylinders to regulate the temperature of the system. All experiments have been conducted at 298.15 K. Titrant is displaced from its bottle to the measurement cell by a peristaltic pump. The feed tube dips into the cell to inject titrant in the

vicinity of the resonator. Mass change is monitored during pumping by placing the titrant bottle on a balance.

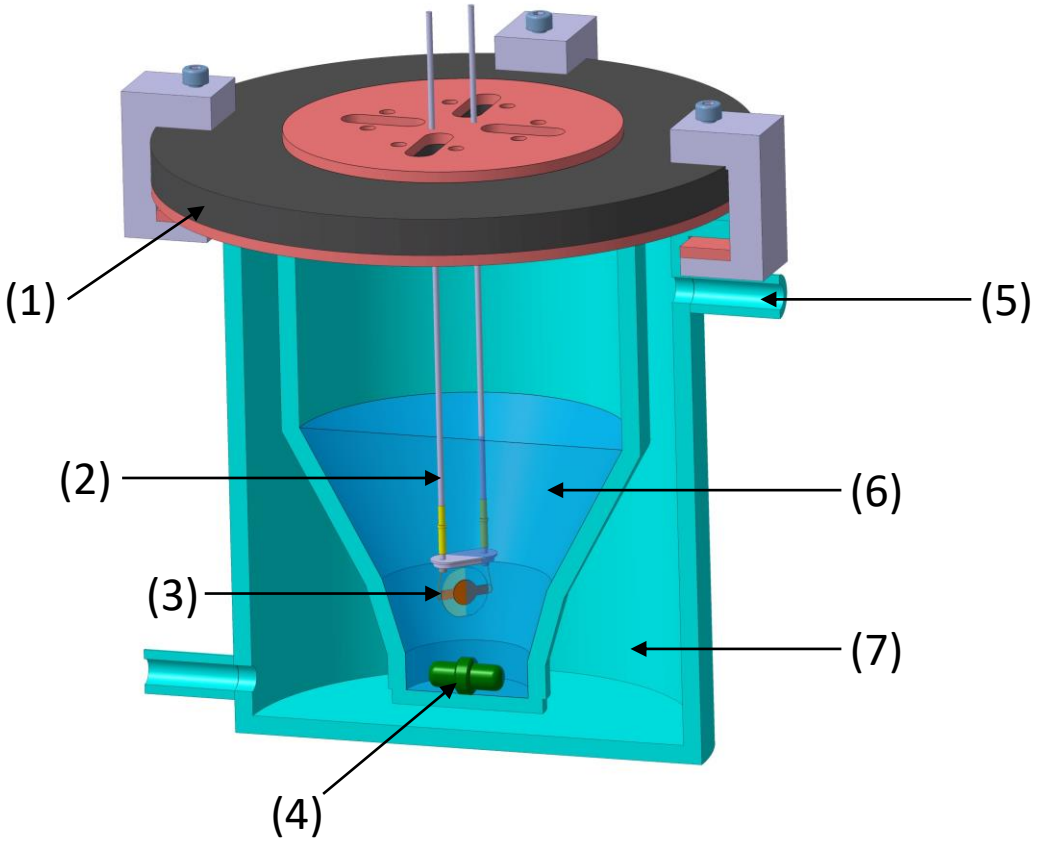

Figure 1. Scheme of the titration cell: (1) sealing cap, (2) electrical connector pins, (3) QCR, (4) magnetic stirring bar, (5) flow line for heat-carrier fluid circulation, (6) liquid solution, (7) double wall glass cyclinder.

2.2.2. High-pressure device. The apparatus is built around a PVT automatic moving piston cell, whose compression chamber is illustrated in Figure 2, and which allows working in the pressure range 0-100 MPa and from 273.15 to 393.15 K. The pressure inside the cell is controlled by a moveable piston and is measured by a pressure transducer directly in contact with the fluid inside the PVT cell. Calibration is performed as a function of temperature against a reference pressure sensor, leading to an error in pressure measurement of less than 0.05 MPa in the experimental pressure range 0.1-100 MPa. The temperature is measured by a platinum

resistance sensor inserted in a thermowell accomodated inside the cell, with an uncertainty better than 0.1 K. Two HP electrical feedthroughs allow the QCR to be used in high pressure conditions and two spherical Teflon-coated magnetic stirrers externally driven by a rotating magnet allow in situ stirring inside the cell. This device has been used for isothermal constant mass expansion experiments.

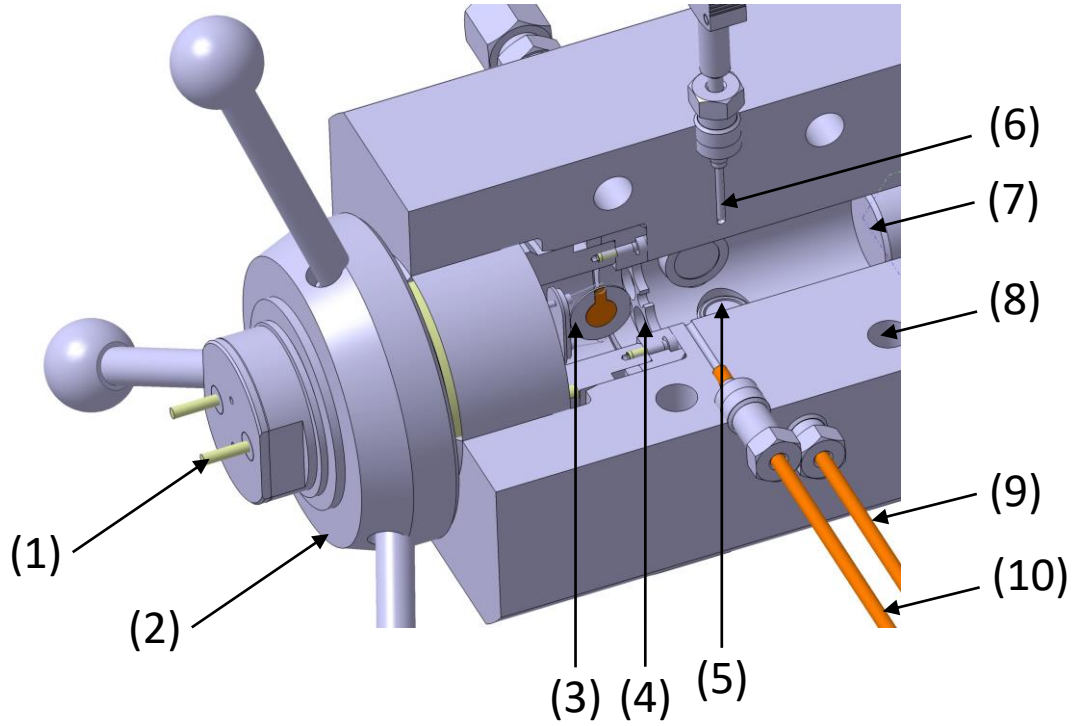

Figure 2. Scheme of the PVT measurement cell: (1) electrical connector pins, (2) high pressure plug, (3) QCR, (4) protective grid, (5) pressure transducer, (6) temperature probe, (7) mobile piston, (8) hole for heat-carrier fluid circulation, (9) flow line for gas injection, (10) flow line for solution injection.

2.2.3. QCR sensor. In both devices, a highly polished AT-cut quartz crystal with a nominal frequency of 3 MHz is used as a sensor. It is connected to a network analyzer that records the complex scattering parameters S_{11}. The conductance G and susceptance B are then calculated according to the following relation:

$$G + iB = \frac{1}{Z_0}\frac{1-S_{11}}{1+S_{11}} \quad (1)$$

where Z_0 is the characteristic impedance of the network analyzer, which is equal to 50 Ω. For odd harmonics ranging from 1 to 11, the conductance spectra recorded using 1601 points around a maximum allow determining both the resonance frequencies f, with an uncertainty of 4 Hz and half-band-half-widths Γ, with an error of less than 5 Hz, by noting the maximum and the bandwidth at half-maximum of the conductance spectrum. The shifts in resonance frequency Δf and half-band-half-width ΔΓ from the values measured in vacuum at the same temperature are then evaluated.

2.3. Sample preparation. A C5Pe + toluene solution was prepared by dissolving 25 mg of C5Pe with 500 mL of toluene (corresponding to a mass concentration of 0.05 g/L), put in ultrasonic bath for 10 min and agitated for 24 hours. This concentration was chosen because it is close to the saturation concentration of C5Pe in toluene. Prior to carrying out any measurement, it was checked by microscopy that the C5Pe sample was well dissolved in toluene. In addition, ^{1}H NMR analysis showed that the positions of peak clusters in the spectrum of a solution C5Pe + $CDCl_3$ measured with a 400 MHz spectrometer were similar to those obtained from a reference spectrum, which revealed that C5Pe sample had not changed from the time it was synthesized. The ^{1}H NMR spectrum can be found in the Supplementary Material.

2.4. Experimental procedure.

2.4.1. Titration experiments. A volume of 19 cm^3 of solution is transferred in the titration cell and the sensor is then immersed in the C5Pe/toluene solution, while the solution is kept agitated thoroughly by the stirrer in the bottom of the cell. A period of 2 hours is generally required for the resonance frequency of the sensor to reach a stable value due to adsorption kinetic and film

formation occurring on the sensor surface. Once steady state is reached, *n*-heptane titration starts with a flow rate of 0.25 g/min.

2.4.2 Pressure scanning experiments. A given amount of solution is transferred at atmospheric pressure to the PVT cell at 298.15 K. Different volumes of compressed methane are then injected into the cell and for each methane molar fraction, successive isothermal constant mass expansion experiments are performed on the same mixture in order to measure the bubble point pressure of the system and to examine if destabilization may occur during depressurization. The bubble point pressure of each system is determined by noting a rupture in both resonance frequency and dissipation curves[49] which coincides with the sharp break observed in the pressure-volume data that is also recorded.

3. THEORY

In a model developed in a previous work,[61] a real QCR immersed in a Newtonian liquid is considered as an ideal sensor with smooth surfaces coated with a thin elastic layer of thickness h_{layer}. The presence of this virtual layer takes into account all the interfacial factors occurring at the electrode-solution interface, including adsorption of molecules on the resonator surface, slippage and roughness. By assuming an asphaltene solution as a Newtonian liquid and by considering additivity of mass deposition on electrode surface with interfacial phenomena, the shifts in resonance frequency $\Delta f_{n,load}$ and half-band-half-width $\Delta\Gamma_{n,load}$ caused by the QCR immersion can be expressed as a linear combination of Sauerbrey and Kanazawa type terms :

$$\Delta f_{n,load} = -n2C_m\rho_D\left(h_{layer} + h_D\right) - \sqrt{n}\frac{C_m}{\sqrt{\pi f_0}}\sqrt{\rho_l\eta_l} \qquad (2)$$

$$\Delta\Gamma_{n,load} = \sqrt{n}\frac{C_m}{\sqrt{\pi f_0}}\sqrt{\rho_l\eta_l}(1+R) \qquad (3)$$

where ρ_D and h_D represent the density and the thickness of the deposited asphaltene layer on electrode surface, h_{layer} is the theoretical thickness of the layer that accounts for interfacial phenomena, n is the overtone number, f_0 is the fundamental resonant frequency of the quartz

resonator in vacuum, ρ_l and η_l are the density and viscosity of the contacting solution, and C_m is the Sauerbrey's coefficient.

$$C_m = 2\frac{f_0^2}{\sqrt{\rho_q \mu_q}} \quad (4)$$

In this expression, ρ_q and μ_q are the density and shear modulus of quartz, respectively. The parameter R that appears in the half-band-half-width expression (eq 3) is a dimensionless coefficient related to the surface morphology through the rheological properties of the virtual layer, and is independent of pressure.[51] In this model, as the thickness h_{layer} can appear negative if slipping of molecules is dominant over adsorption or mass deposition phenomena, its value should be determined and serve as a correction term to obtain the real thickness of the deposited asphaltene layer h_D.

4. RESULTS AND DISCUSSION

4.1. Precipitation of C5Pe and asphaltenes with heptane. Shifts in frequency corresponding to different harmonics recorded during titration of the C5Pe/toluene (0.05 g/L) system are presented in Figure 3. For each harmonic, titration curves first increase because of the reduction in viscosity caused by the addition of *n*-heptane, as observed with the titration of pure toluene presented in a previous work.[38] At a *n*-heptane molar percentage of around 40%, the shifts in frequency start deviating from the linear behaviour and then start decreasing from around 55% of titrant content. Typical curves of the changes in half-band-half-width versus the molar fraction of the added titrant since the beginning of the titration experiment are given for various overtones in Figure 4. In the same way as frequency curves, changes in dissipation curves are divided into two parts. In the first part, dissipation smoothly decreases because of *n*-heptane dissolution, whereas, in the second part, it increases as a result of C5Pe precipitation.

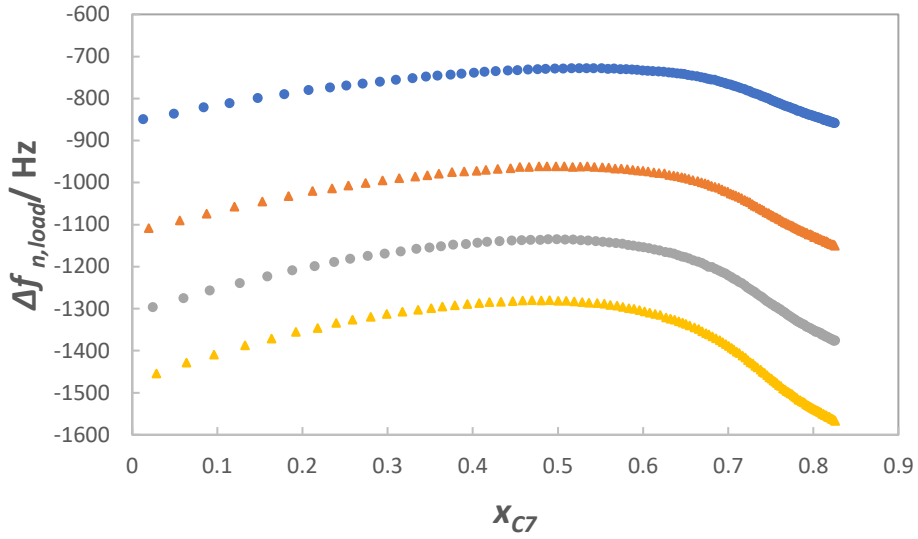

Figure 3. Shifts in resonance frequency of different harmonics recorded as a function of heptane molar fraction during titration of the C5Pe + toluene (0.05 g/L) system at 298.15 K and 0.1 MPa. ●, 3rd harmonic; ▲, 5th harmonic; ■, 7th harmonic; ●, 9th harmonic.

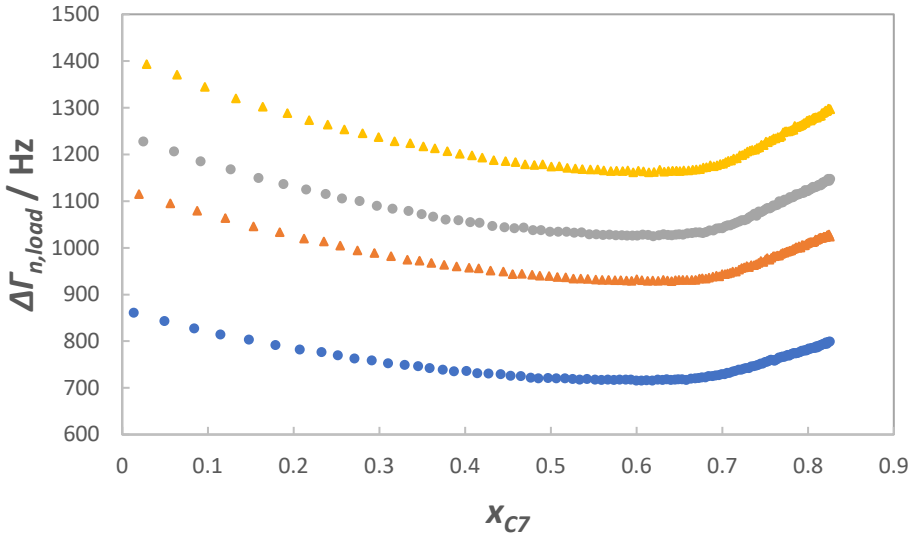

Figure 4. Changes in half-band-half-width of different harmonics recorded as a function of heptane molar fraction during titration of the C5Pe + toluene (0.05 g/L) system at 298.15 K and 0.1 MPa. ●, 3rd harmonic; ▲, 5th harmonic; ●, 7th harmonic; ▲, 9th harmonic.

From this behaviour, it can be concluded that C5Pe in solution destabilize and form aggregates. This phenomenon is probed either by the change in the frequency shift or the bandwidth increase of the QCR immersed in solution. In order to compare these observations with the QCR response to asphaltene destabilization, a titration experiment was carried out in the same conditions of temperature and titration kinetics with a real asphaltene/toluene system. By following the same protocol as for the C5Pe/toluene system, a solution composed of PetroPhase 2017 asphaltenes and toluene with the same mass concentration of 0.05 g/L was prepared and *n*-heptane titration experiment was repeated. Figure 5 reveals that the titration curves in frequency on the different harmonics deviate to the normal behaviour at a lower *n*-heptane molar fraction (i.e. 30%) than for the C5Pe/toluene solution whereas the titration curves in dissipation do not present a change as sharp as for the model molecule (Figure 6). In order to obtain a precise value of the heptane/toluene ratio at which asphaltene precipitation starts, the dilution effect is subtracted from titration curves by adjusting three parameters of Grunberg-Nissan-type equations to fit the first parts of both frequency and dissipation titration curves.[38] The frequency titration curves for the different systems are reported for the third harmonic in Figure 7 and for the seventh harmonic in Figure 8. It can be observed from these figures that in the first part of the experiment (i.e. from 0 to 20% of *n*-heptane content) the titration curve for C5Pe matches the one for asphaltenes on the third harmonic, whereas on the seventh harmonic, curves deviate from each other. According to the QCR model, this behaviour could probe either a change in the nature of the interfacial layer or in the density-viscosity product of the contacting solution. Then it can be seen graphically that the amplitude of the frequency shift on the third harmonic from 20 to 82% heptane molar fraction is higher (355 Hz) for the asphaltenes + toluene system than for the C5Pe dissolved in toluene (75 Hz) at the same mass concentration of 0.05 g/L. The dissipation titration curves of the different systems that are displayed in Figure 9 show on the one hand a higher value of half-band-half-width on the third overtone for

asphaltenes compared to C5Pe and toluene, which means that the deviation observed in the frequency shift on the higher overtones when titration starts is mainly due to a change in the fluid properties of the asphaltenes solution. On the other hand, Figure 9 reveals that half-band-half-width increases by 80 Hz from 65 to 82% *n*-heptane mass fraction for C5Pe/toluene system whereas it remains constant in this concentration range for asphaltenes/toluene. Also it can be seen from Figure 10 that the ratio $-\Delta f_{n,load}(1+R)/\Delta\Gamma_{n,load}$ calculated on the third harmonic has a value comprised between 1 and 1.2 during the whole titration experiment for C5Pe, whereas it continuously rises up to 1.65 for asphaltenes. This clearly shows that, according to the model, the main phenomena observed for C5Pe by the QCR is an increase in the viscosity, meaning that C5Pe destabilize to form aggregates or clusters that look stable in suspension in the solution, whereas for asphaltenes the main observation is mass deposition, where asphaltenes destabilize to form clusters that diffuse to the electrode surface. Each titration experiment was repeated at least three times and the difference in behaviour between the systems was higher than the accuracy and the reproducibility of the data, which confirmed the phenomena observed. The higher magnitude of the sensor response to destabilization in the case of the asphaltenes can be related to the polydispersity of the samples. As PetroPhase 2017 asphaltenes present a high level of polydispersity,[53] their precipitation occurs in a range of solvation conditions whereas the precipitation of C5Pe takes place at a specific heptane volume fraction since it is a well-defined molecule. This could explain why addition of more heptane is needed to cause destabilization of C5Pe than in the case of Petrophase 2017 asphaltenes.

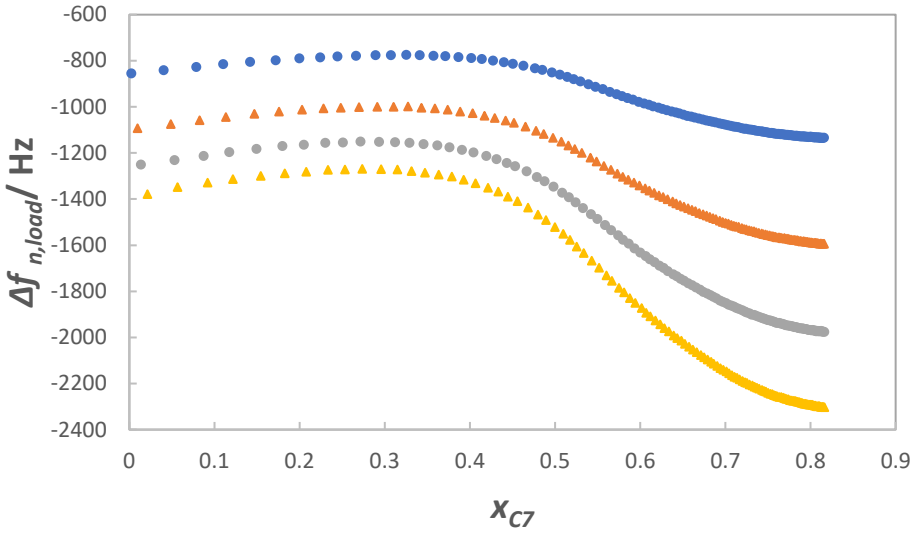

Figure 5. Shifts in resonance frequency of different harmonics recorded as a function of heptane molar fraction during titration of the PetroPhase 2017 asphaltenes + toluene (0.05 g/L) system at 298.15 K and 0.1 MPa. ●, 3rd harmonic; ▲, 5th harmonic; ■, 7th harmonic; ●, 9th harmonic.

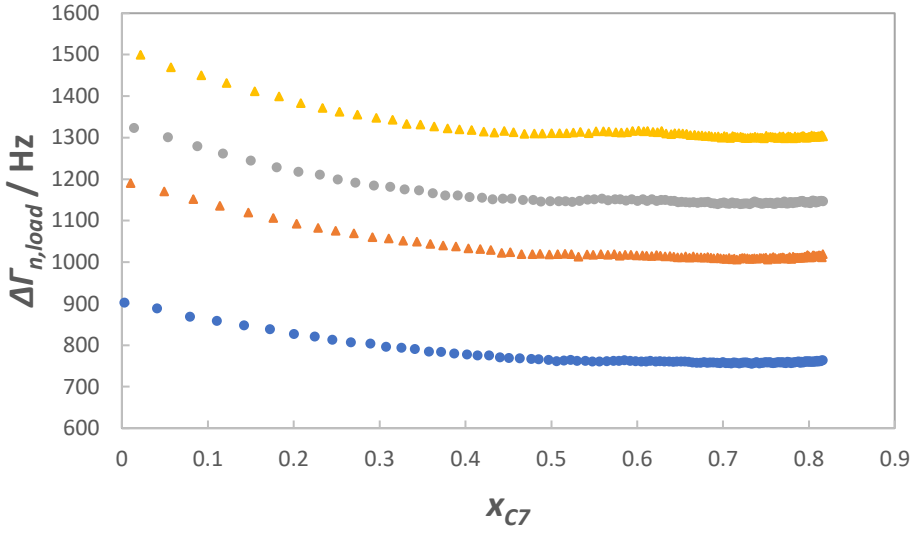

Figure 6. Changes in half-band-half-width of different harmonics recorded as a function of heptane molar fraction during titration of the PetroPhase 2017 asphaltenes + toluene (0.05 g/L) system at 298.15 K and 0.1 MPa. ●, 3rd harmonic; ▲, 5th harmonic; ■, 7th harmonic; ●, 9th harmonic.

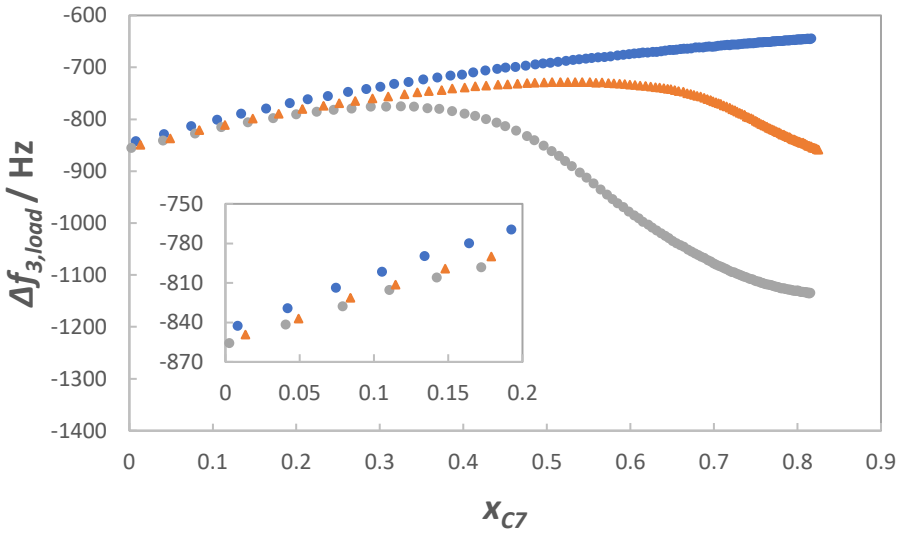

Figure 7. Shifts in resonance frequency of the third harmonic recorded as a function of heptane molar fraction during titration of the different systems at 298.15 K and 0.1 MPa. ▲, C5Pe + toluene (0.05 g/L); ●, PetroPhase 2017 asphaltenes + toluene (0.05 g/L); ●, pure toluene.

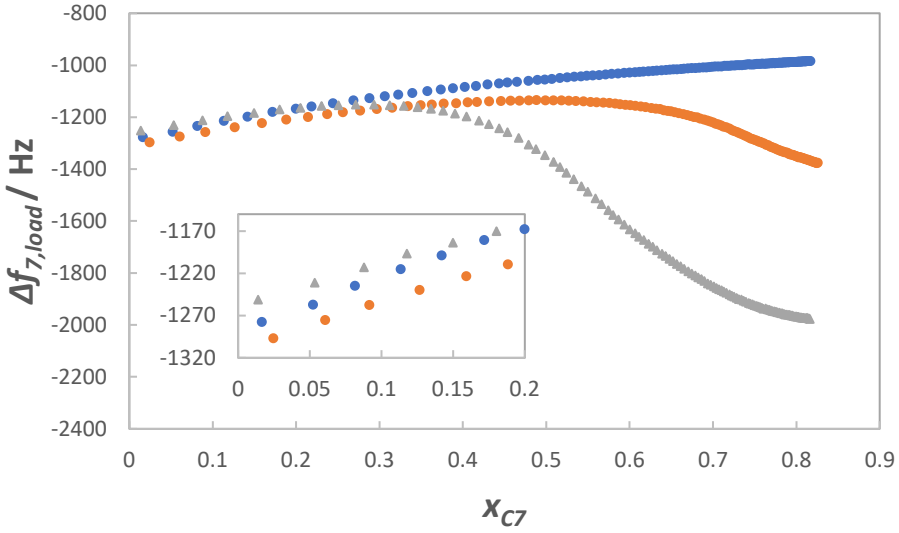

Figure 8. Shifts in resonance frequency of the seventh harmonic recorded as a function of heptane molar fraction during titration of the different systems at 298.15 K and 0.1 MPa. ▲, C5Pe + toluene (0.05 g/L); ●, PetroPhase 2017 asphaltenes + toluene (0.05 g/L); ●, pure toluene.

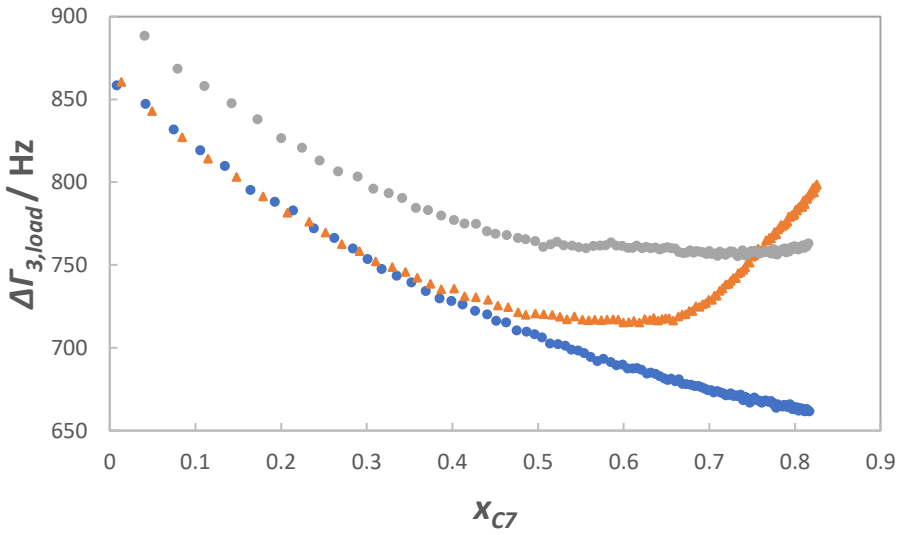

Figure 9. Changes in half-band-half-width on the third harmonic recorded as a function of heptane molar fraction during titration of the different systems at 298.15 K and 0.1 MPa. ▲, C5Pe + toluene (0.05 g/L); ●, PetroPhase 2017 asphaltenes + toluene (0.05 g/L); ●, pure toluene.

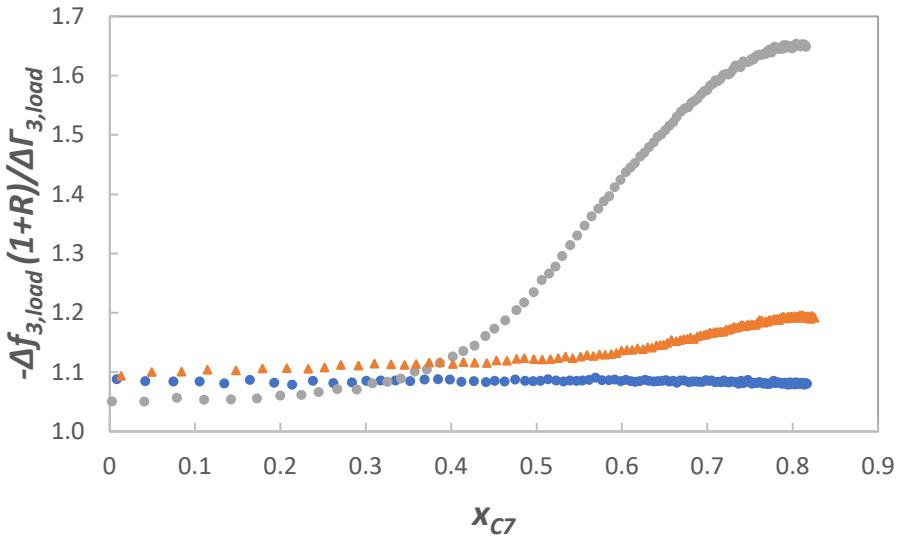

Figure 10. Evolution of the parameter $-\Delta f_{3,load}(1+R)/\Delta\Gamma_{3,load}$ calculated on the third harmonic as a function of heptane molar fraction during titration of the different systems at 298.15 K and 0.1 MPa. ▲, C5Pe + toluene (0.05 g/L); ●, PetroPhase 2017 asphaltenes + toluene (0.05 g/L); ●, pure toluene.

From frequency shifts measured on the 3rd, 5th and 7th overtones, the values of the deposited layer thickness h_D for the different systems were calculated using eq 2, whereas density-viscosity products were determined from half-band-half-width measurements and eq 3. The obtained results confirm the sharper increase in the density-viscosity product for solution containing C5Pe than for solution with asphaltenes (Figure 11) when destabilization occurs whereas the apparent thickness (Figure 12) reaches higher values for the asphaltene solution than for C5Pe in solution, meaning that the deposition process is more significant with asphaltenes than with C5Pe. Thickness values of the deposited layer on QCR surface at different heptane molar fractions for the two systems are reported in Table 1. It can be noted that the values of a few nanometers obtained for the adsorbed asphaltene film thickness are consistent with the values measured form SANS or neutron reflectometry studies.[62-64] However, as these values were measured in good solvent (toluene) and not in precipitating conditions, larger thickness values in the case of *n*-heptane addition were expected. The very weak concentration of solute in the system (0.05 g/L) and the short time of titration experiment (90 min) can explain the low amount of deposited particles on the electrode surface.

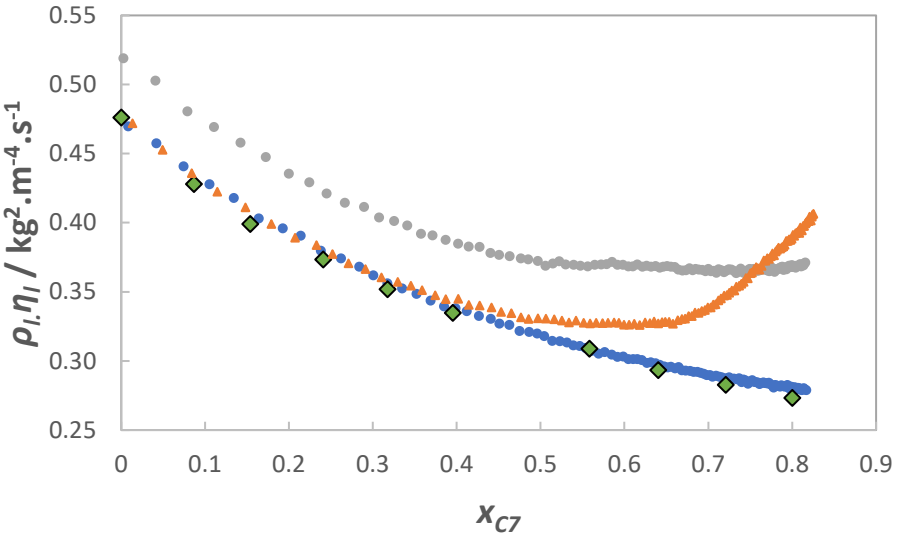

Figure 11. Changes in density-viscosity product as a function of heptane molar fraction calculated from half-band-half-width measurements during titration of the different systems at

298.15 K and 0.1 MPa. ▲, C5Pe + toluene (0.05 g/L); ●, PetroPhase 2017 asphaltenes + toluene (0.05 g/L); ●, pure toluene; ♦, Data of Iloukhani et al.[65]

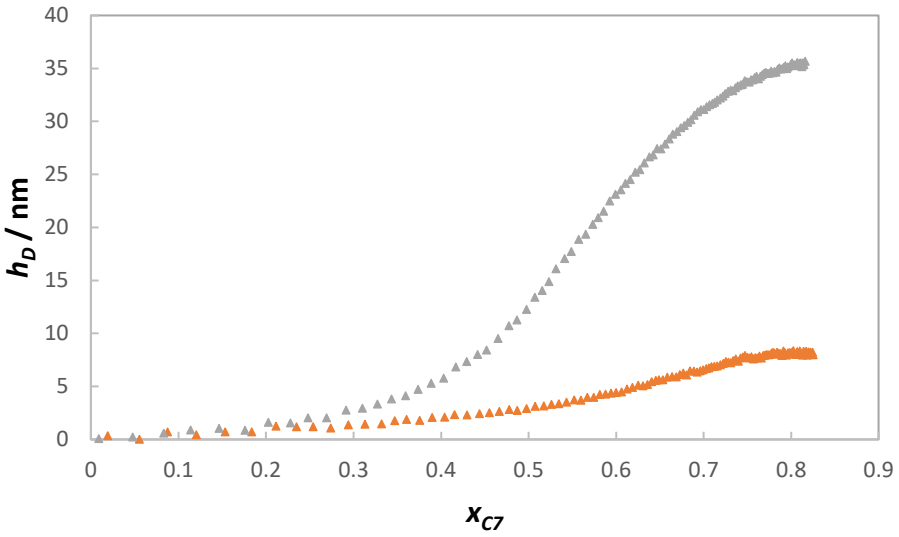

Figure 12. Changes in deposited layer thickness h_D as a function of heptane molar fraction during titration of the different systems at 298.15 K and 0.1 MPa. ▲, C5Pe + toluene (0.05 g/L); ●, PetroPhase 2017 asphaltenes + toluene (0.05 g/L).

	h_D at x (mol %) C_7 / nm			
	50 %	60 %	70 %	80 %
C5Pe	3	4	7	8
Asphaltenes	13	23	31	35

Table 1. Thickness values of deposited layer on QCR surface during *n*-heptane titration of C5Pe/toluene and Petrophase 2017 asphaltenes/toluene systems at 298.15 K and 0.1 MPa.

4.2. Precipitation of C5Pe and asphaltenes with methane. This investigation began by a series of successive constant mass expansion experiments performed at a constant rate of pressure drop of 0.4 MPa/min with 21, 40, 50, 59 and 65% of CH_4 content (in mol %) in a

sample of 18.5 g of C5Pe/toluene solution at 0.05 g/L. For all the mixtures, a V-shape curve in the $\Delta\Gamma_{3,load}$ versus P plot is obtained (Figure 13). The decrease in half-band-half width from the start of the pressure scanning experiment until the bubble point corresponds to the monotonous decrease of the density-viscosity product of the system as the pressure drops. By contrast, as shown in Figure 14, a Λ-shape curve is observed in the $\Delta f_{3,load}$ versus P plot for mixtures containing 21% and 40%, whereas for the other systems containing 50, 59 and 65%, a decrease in $\Delta f_{3,load}$ is observed before reaching the bubble point. For the mixture containing 65%, a drop of 120 Hz is observed between the depressurization onset (80 MPa) and the bubble point pressure (40.7 MPa). All these results show that the sensor detects the presence of interfacial phenomena that could change the resonance properties of the QCR during decompression of the C5Pe/toluene + methane system, when the molar fraction of CH_4 is above 50%.

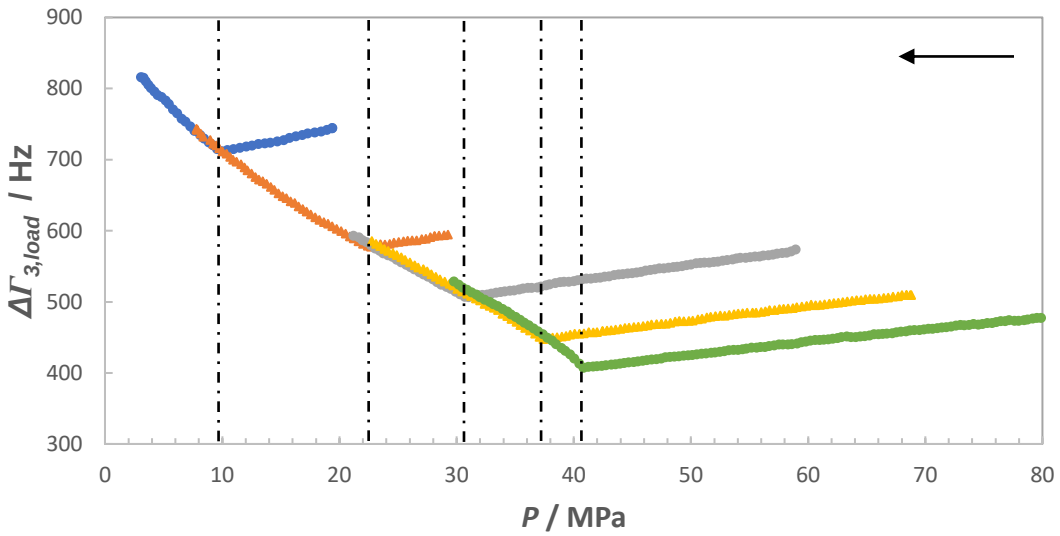

Figure 13. Changes in half-band-half-width $\Delta\Gamma_{3,load}$ for the third overtone of the acoustic wave sensor immersed in C5Pe/toluene (0.05 g/L) + CH_4 systems with various contents of CH_4 (in

mol %) during constant mass expansion at 298.15 K. ●, 21%; ▲, 40%; ●, 50%; ▲, 59%; ●, 65%; — · —, bubble point pressures.

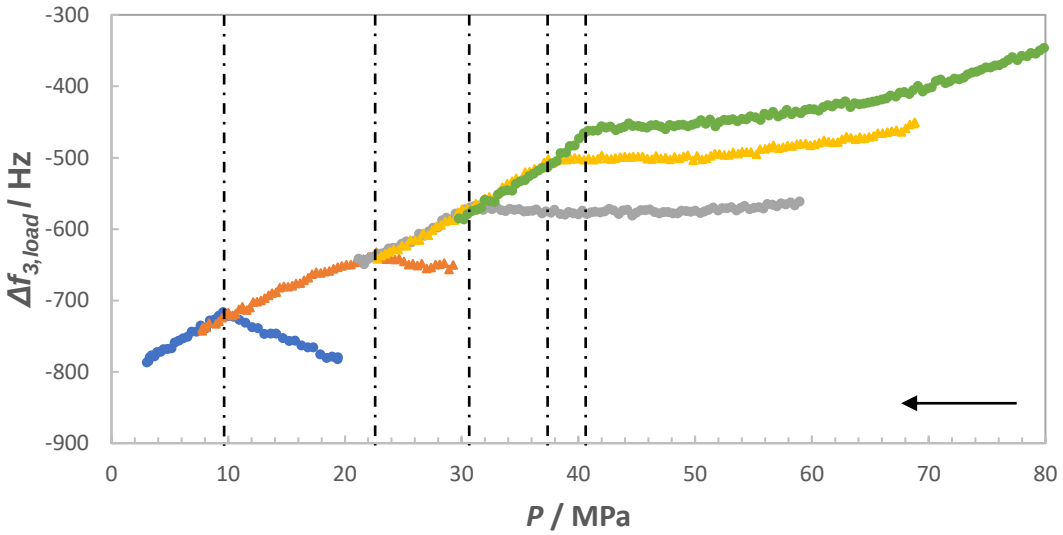

Figure 14. Shifts in resonance frequency $\Delta f_{3,load}$ for the third overtone of the acoustic wave sensor immersed in C5Pe/toluene (0.05 g/L) + CH_4 systems with various contents of CH_4 (in mol %) during constant mass expansion at 298.15 K. ●, 21%; ▲, 40%; ●, 50%; ▲, 59%; ●, 65%; — · —, bubble point pressures.

In order to verify that the variations observed in the frequency shifts are caused by C5Pe precipitation, the reference system pure toluene + methane in the absence of C5Pe was studied under the same conditions. The resulting curves (Figures 15 and 16) reveal that for all the toluene + CH_4 mixtures the sensor response to fluid decompression exhibits the same behaviour as that observed with C5Pe/toluene + CH_4. Consequently, the decrease in frequency from 50% of CH_4 content in the liquid phase means that the sensor doesn't probe at this point a change in the density-viscosity product of the contacting solution but a change occurring at the electrode-solution interface. This corresponds to a combination of two effects. The first one is related to the continuous adsorption of molecules in the cavities and pores of the QCR rough surface when

the pressure of the contacting liquid decreases and the second one is linked to the decrease in the slippage of the fluid with pressure.[51] This behaviour can be avoided if the QCR is immersed for a longer time, i.e., several hours, at the equilibrium pressure in order to allow the complete formation of the adsorbed layer on the electrode surface. However due to the mechanical design of the high pressure cell, this option is not practically feasible and depressurization is generally started only a few minutes after reaching the equilibrium pressure, and thus not allowing sufficient time for the interfacial layer to form. As the same trend was observed for the C5Pe/toluene + CH_4 system and that the calculation of the interfacial layer thickness showed the same values compared to pure toluene + CH_4, it can be concluded that no significant precipitation of C5Pe with methane occurs in the different systems investigated with CH_4 contents ranging from 0 to 65 %.

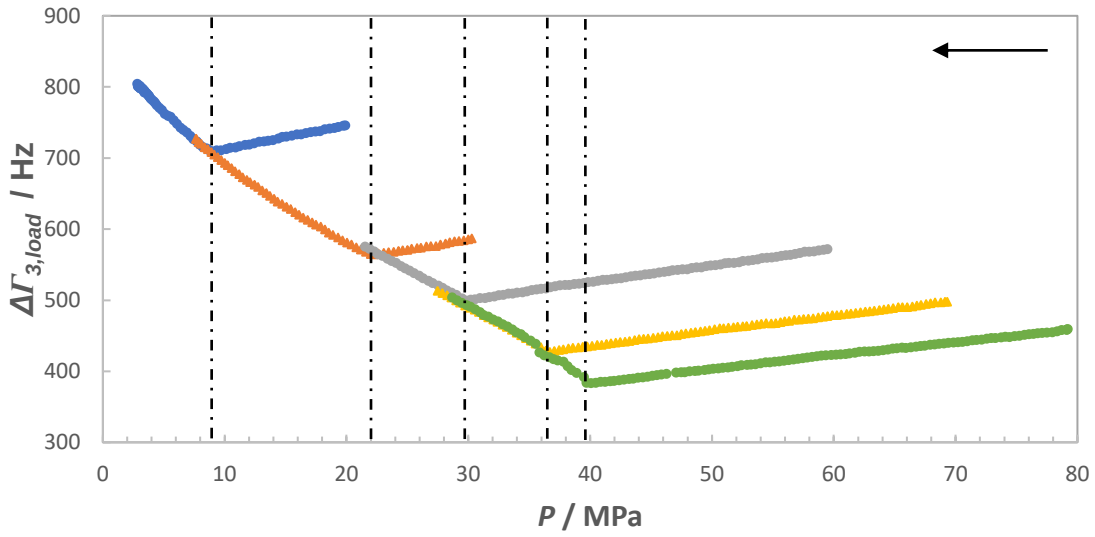

Figure 15. Changes in half-band-half-width $\Delta\Gamma_{3,load}$ for the third overtone of the acoustic wave sensor immersed in pure toluene + CH_4 systems with various contents of CH_4 (in mol %) during constant mass expansion at 298.15 K. ●, 20%; ▲, 40%; ●, 50%; ▲, 59%; ●, 65%. —·—, bubble point pressures.

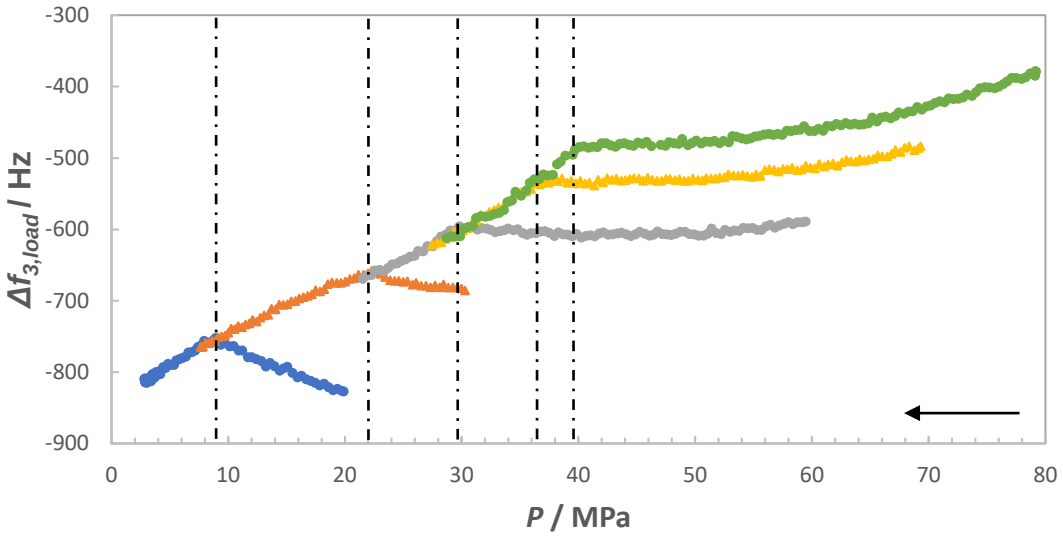

Figure 16. Shifts in resonance frequency $\Delta f_{3,load}$ for the third overtone of the acoustic wave sensor immersed in pure toluene + CH_4 systems with various contents of CH_4 (in mol %) during constant mass expansion at 298.15 K. ●, 20%; ▲, 40%; ●, 50%; ▲, 59%; ●, 65%; —·—, bubble point pressures.

The same experiments were then repeated with a PetroPhase 2017 asphaltenes + toluene solution at 0.05 g/L. Different constant mass expansion experiments were performed after injecting the same amounts of methane as in the previous experiments. It can be seen in Figures 17 and 18 that the sensor response to immersion in the asphaltenes solution for both half-band-half width and resonance frequency is different from that observed for the systems pure toluene + CH_4 and C5Pe/toluene + CH_4. In order to distinguish between rheological changes in the QCR surrounding medium and mass deposition phenomena, the thickness values h_D were calculated and plotted as a function of pressure in Figure 19. Observation of this figure indicates that the deposited layer thickness tends to increase with the CH_4 molar fraction, reaching a maximum of 20 nm around 40 MPa at 65 % of CH_4 content. This trend matches the results obtained at atmospheric pressure presented in Figures 11 and 12, where higher density-viscosity

products and mass deposition were observed for asphaltenes/toluene than C5Pe/toluene up to 65% of heptane molar fraction.

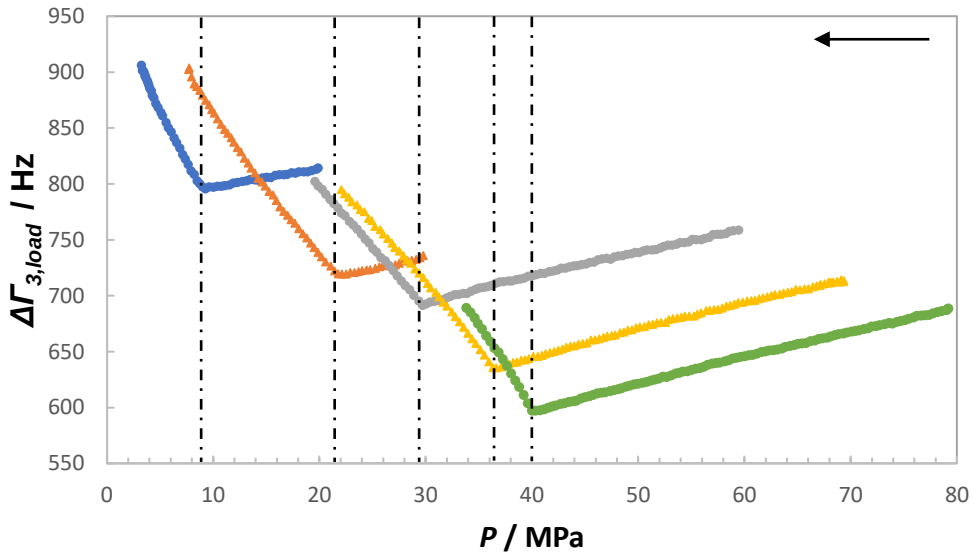

Figure 17. Changes in half-band-half-width $\Delta\Gamma_{3,load}$ for the third overtone of the acoustic wave sensor immersed in PetroPhase 2017 asphaltenes/toluene (0,05 g/L) + CH_4 systems with various contents of CH_4 (in mol %) during constant mass expansion at 298.15 K. ●, 20%; ▲, 40%; ●, 50%; ▲, 59%; ●, 65%; — · —, bubble point pressures.

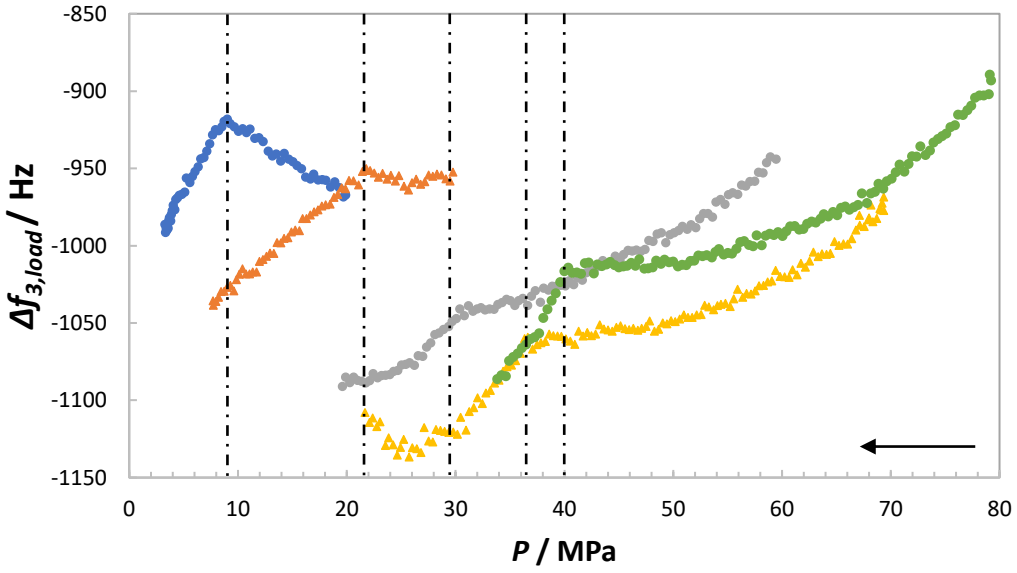

Figure 18. Shifts in resonance frequency $\Delta f_{3,load}$ for the third overtone of the acoustic wave sensor immersed in PetroPhase 2017 asphaltenes/toluene (0,05 g/L) + CH_4 systems with various contents of CH_4 (in mol %) during constant mass expansion at 298.15 K. ●, 20%; ▲, 40%; ●, 50%; ▲, 59%; ●, 65%; — · —, bubble point pressures.

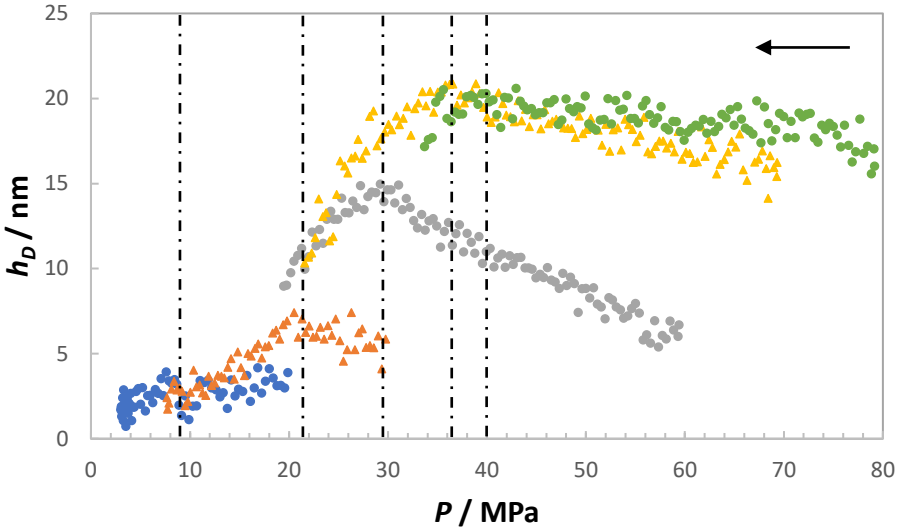

Figure 19. Changes in deposited layer thickness for PetroPhase 2017 asphaltenes (0.05 g/L) + CH_4 systems with various contents of CH_4 (in mol %) during constant mass expansion at 298.15 K. ●, 20%; ▲, 40%; ●, 50%; ▲, 59%; ●, 65%; — · —, bubble point pressures.

Therefore, as no significant C5Pe flocculation phenomena was observed up to 65% of methane concentration, new samples were prepared to investigate if higher methane content would induce more C5Pe flocculation and/or deposition on the quartz resonator surface. As higher volumes of methane need to be injected in the PVT cell in order to reach such high molar gas fractions and due to the limited volume of the device, the initial amount of sample introduced in the cell was reduced to 10 g for preparing the mixture with 72% of CH_4 content and to 9 g for 80% and 85% CH_4, which represents half the quantity introduced in the previous experiments. The calculated values of $\rho_l \eta_l$ at 72 mol % of CH_4 presented in Figure 20 reveal a higher value of the density-viscosity product of the contacting C5Pe/toluene + CH_4 solution

compared to pure toluene + CH_4 mixture with the same CH4 content at the beginning of the depressurization ramp (90 MPa). Then one can note an increase in $\rho_l \eta_l$ until 71 MPa, followed by a decrease up to the bubble point. This behavior means that C5Pe molecules are already precipitated when depressurization starts, causing an increase in the density-visosity product of the solution until C5Pe flocs reach their final size. For the asphaltenes/toluene system, it can be observed that $\rho_l \eta_l$ decreases with pressure in the same way as the pure toluene/CH_4 system, although it starts from a higher value, which means that asphaltenes are also precipitated at the equilibrium pressure of 90 MPa. Calculation of h_D reveals that the deposited layer thickness reaches a value of 20 nm for asphaltenes/toluene whereas it doesn't exceed 5 nm in the case of C5Pe/toluene (Figure 21). The same behaviour was observed during experiments conducted with 80% and 85% of CH_4 content (in mol %). These results confirm the observations made at atmospheric pressure, i.e., on the one hand low adsorption on the quartz resonator surface but significant increase in the density-viscosity product of the contacting C5Pe/toluene solution, and on the other hand higher adsorption and lower increase in density-viscosity product for asphaltenes/toluene solution. Also, it can be noted that the maximum values of the adsorbed layer thickness during depressurization with methane are lower than those obtained during continuous titration experiments with heptane. This behaviour can be explained by two main reasons. The first one comes from the difference in mechanical stirring mode between the two devices. In the atmospheric pressure apparatus, the rotation at high speed of the magnetic bar at the bottom of the titration cell would be more efficient for the aggregates to diffuse to the QCR surface, compared to the movement of the two spherical magnetic stirrers which would only provide limited stirring of the mixture, and therefore would not be optimal for particle deposition on the sensor surface. The second reason is the lower amount of studied sample from 72% of CH_4 molar content. Indeed as the injected volume of solution is reduced by half in the

high pressure cell compared to the titration cell, the quantity of molecules that would precipitate and adsorb on the quartz surface is all the more reduced.

Finally, the bubble point pressures determined from the *P,v* curves for the different systems are reported in Table 2. According to the depressurization rate value of 0.4 MPa/min, the experimental uncertainty taken for the bubble point pressure measurement is 0.5 MPa. All the resulting values appear to fall within the range of this measurement uncertainty. To our knowledge, no experimental data for the liquid-vapor phase transition of the methane + toluene system along the 298.15 K isotherm are available in the literature. However, graphical representation reveals that our measurements are in good agreement with the trend of the available literature data along other isotherms,[67-69] especially near the critical region, as shown in Figure 22. This study confirms how suitable the QCR technique is to work with the different systems C5Pe/toluene + CH_4 and PetroPhase asphaltenes 2017/toluene + CH_4. Moreover, the C5Pe and asphaltene stability-instability phase boundaries were not detected during these constant mass expansion experiments and therefore were not reported in Table 2.

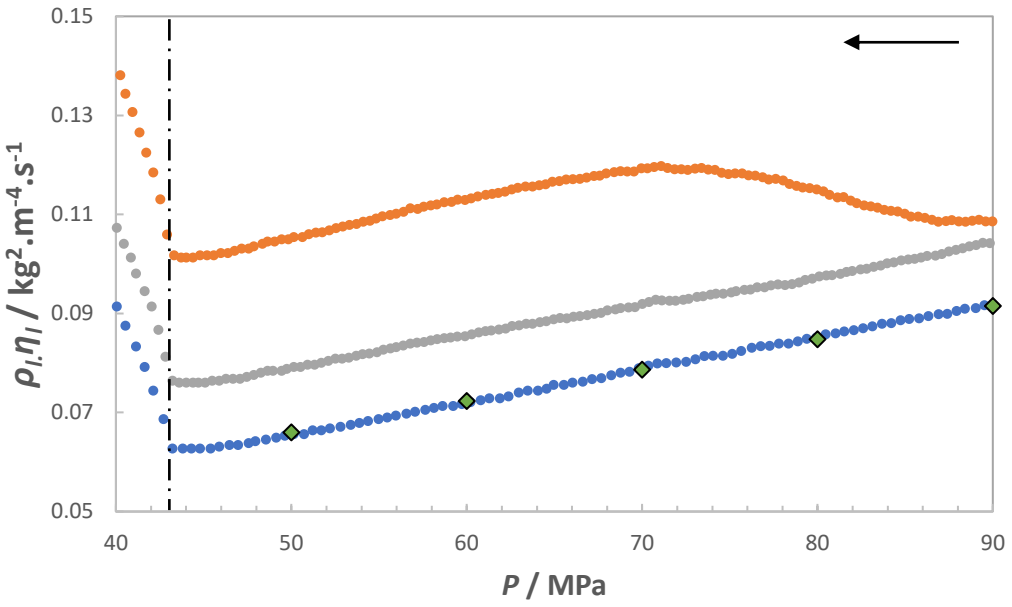

Figure 20. Changes in density-viscosity product calculated from half-band-half-width measurements on the third overtone for the different systems with 72 mol % of CH_4 during constant mass expansion at 298.15 K. ▲, C5Pe/toluene (0.05 g/L); ●, PetroPhase 2017 asphaltenes/toluene (0.05 g/L); ●, pure toluene; ♦, Data of Baylaucq et al.[66]; — · —, bubble point pressure.

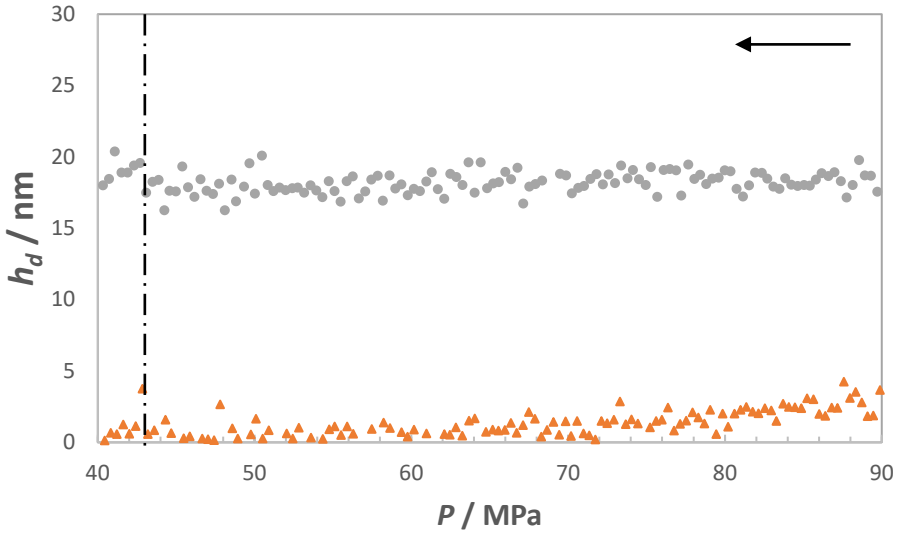

Figure 21. Changes in deposited layer thickness h_D for the different systems with 72 mol % of CH_4 during constant mass expansion at 298.15 K. ▲, C5Pe/toluene (0.05 g/L); ●, PetroPhase 2017 asphaltenes/toluene (0.05 g/L); — · —, bubble point pressure.

System	CH_4 % (mol %)	Bubble point (MPa)
C5Pe	21.7	9.8
Asphaltenes	20.7	8.9
Toluene	20.3	8.9
C5Pe	39.8	22.5
Asphaltenes	40.3	21.7
Toluene	40.3	22.0
C5Pe	50.1	30.6
Asphaltenes	50.3	29.6
Toluene	50.3	29.8
C5Pe	59.0	37.3
Asphaltenes	59.2	36.4
Toluene	59.2	36.5
C5Pe	65.1	40.7
Asphaltenes	65.5	40.0
Toluene	65.5	39.7
C5Pe	72.0	43.4
Asphaltenes	72.0	43.2
Toluene	72.2	43.1
C5Pe	80.1	43.7
Asphaltenes	80.0	44.0
Toluene	80.2	43.6
C5Pe	85.0	43.2
Asphaltenes	85.0	43.4
Toluene	85.0	43.5

Table 2. Bubble point pressure values determined for the different systems C5Pe/toluene + CH_4, PetroPhase 2017 asphaltenes/toluene + CH_4 and toluene + CH_4 with various CH_4 contents (in mol %) at 298.15 K.

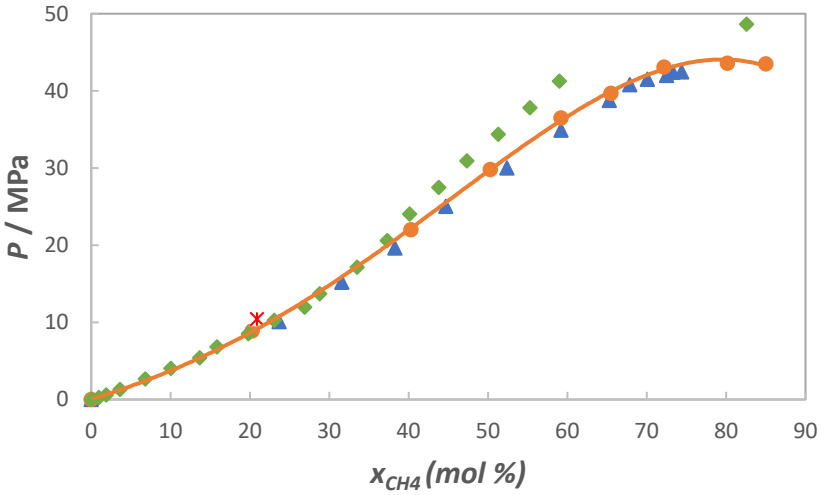

Figure 22. Vapor-liquid equilibrium data for the system methane-toluene: ●, 298.15 K isotherm (present work); ▲, 313.2 K isotherm (Data of Legret et al.[67]); ♦, 277.59 K isotherm (Data of Lin et al.[68]); ∗, 293.15 K isotherm (Data of Hugues et al.[69]).

5. CONCLUSION

In this work the ability of the model compound C5Pe to correctly represent the solution properties of asphaltenes was investigated by an acoustic wave sensor. It has been first demonstrated during a continuous titration experiment at atmospheric pressure that C5Pe molecules dissolved in toluene precipitate upon addition of *n*-heptane, and thus meet the solubility definition of asphaltenes. It has also been shown that the model compound starts to self-associate at a higher heptane molar fraction compared to PetroPhase 2017 extracted asphaltenes. This behaviour has been confirmed by carrying out constant mass expansion experiments with various amounts of injected CH_4. During a pressure scanning, destabilization of C5Pe molecules was only significant for systems containing more than 65% CH_4 whereas

destabilization of extracted asphaltenes was sensed in a wider range of CH_4 content. However, the flocculation of C5Pe was probed by a change in the density-viscosity product of the contacting solution rather than a significant increase of the adsorbed layer on the gold surface. Conversely, the amount of adsorbed PetroPhase 2017 asphaltenes was higher during titration or depressurization. However, as the resonance frequency and dissipation curves did not present significant discontinuities or breaks during depressurization of the different systems, the boundaries of the C5Pe and asphaltene instability domain could not be clearly assessed. The reason that the model compound does not self-associate to the same extent as the extracted asphaltenes could most probably be due to the difference in polydispersity between the two compounds. The C5Pe molecule only represents one subfraction of indigeneous asphaltenes as a whole and because the interactions between different asphaltenes compounds are lacking, the model compound cannot fully address the behaviour of asphaltenes in solution. In the future it would be necessary to test more complex structures to mimic the association behaviour of asphaltenes.

REFERENCES

(1) Leontaritis, K. J.; Ali Mansoori, G. Asphaltene deposition: a survey of field experiences and research approaches. *Journal of Petroleum Science and Engineering* 1988, 1 (3), 229-239.

(2) Thawer, R.; Nicoll, D. C. A.; Dick, G. Asphaltene deposition in production facilities. *SPE Production Engineering* 1990, 5, 475-480.

(3) Subramanian, S.; Simon, S.; Sjöblom, J. Asphaltene precipitation models: A Review. *Journal of Dispersion Science and Technology* 2016, 37 (7), 1027-1049.

(4) Sjöblom, J.; Aske, N.; Harald Auflem, I.; Brandal, O.; Erik Havre, T.; Saether, O.; Westvik, A.; Eng Johnsen, E.; Kallevik, H. Our current understanding of water-in-crude oil

emulsions.: Recent characterization techniques and high pressure performance. *Advances in Colloid and Interface Science* 2003, 100-102, 399-473.

(5) Sjöblom, J.; Simon, S.; Xu, Z. Model molecules mimicking asphaltenes. *Advances in Colloid and Interface Science* 2015, 218 (0), 1-16.

(6) Nordgård, E. L.; Landsem, E.; Sjöblom, J. Langmuir films of asphaltene model compounds and their fluorescent properties. *Langmuir* 2008, 24 (16), 8742-8751.

(7) Nordgård, E. L.; Sørland, G.; Sjöblom, J. Behavior of asphaltene model compounds at W/O interfaces. *Langmuir* 2010, 26 (4), 2352-2360.

(8) Akbarzadeh, K.; Bressler, D. C.; Wang, J.; Gawrys, K. L.; Gray, M. R.; Kilpatrick, P. K.; Yarranton, H. W. Association behavior of pyrene compounds as models for asphaltenes. *Energy Fuels* 2005, 19 (4), 1268-1271.

(9) Rakotondradany, F.; Fenniri, H.; Rahimi, P.; Gawrys, K. L.; Kilpatrick, P. K.; Gray, M. R. Hexabenzocoronene model compounds for asphaltene fractions: Synthesis & characterization. *Energy Fuels* 2006, 20 (6), 2439-2447.

(10) Tan, X.; Fenniri, H.; Gray, M. R. Pyrene derivatives of 2,2′-bipyridine as models for asphaltenes: Synthesis, characterization, and supramolecular organization. *Energy Fuels* 2008, 22 (2), 715-720.

(11) Mohammed, S.; Gadikota, G. The influence of CO_2 on the structure of confined asphaltenes in calcite nanopores. Fuel 2019, 236, 769-777.

(12) Mohammed, S.; Gadikota, G. The role of calcite and silica interfaces on the aggregation and transport of asphaltenes in confinement. Journal of Molecular Liquids 2019, 274, 792-800.

(13) Mohammed, S.; Gadikota, G. Dynamic wettability alteration of calcite, silica and illite surfaces in subsurface environments: A case study of asphaltene self-assembly at solid interfaces. Applied Surface Science 2020, 505, 144516.

(14) Wang, X.; Zhang, R.; Liu, L.; Qiao, P.; Simon, S.; Sjöblom, J.; Xu, Z.; Jiang, B. Interactions of polyaromatic compounds. Part 2. Flocculation probed by dynamic light scattering and molecular dynamics simulation. *Energy Fuels* 2017, 31 (9), 9201-9212.

(15) Nordgård, E. L.; Sjöblom, J. Model compounds for asphaltenes and C80 isoprenoid tetraacids. Part I: Synthesis and interfacial activities. *Journal of Dispersion Science and Technology* 2008, 29 (8), 1114-1122.

(16) Teklebrhan, R. B.; Ge, L.; Bhattacharjee, S.; Xu, Z.; Sjöblom, J. Probing structure-nanoaggregation relations of polyaromatic surfactants: A molecular dynamics simulation and dynamic light scattering study. *The Journal of Physical Chemistry B* 2012, 116 (20), 5907-5918.

(17) Teklebrhan, R. B.; Ge, L.; Bhattacharjee, S.; Xu, Z.; Sjöblom, J. Initial partition and aggregation of uncharged polyaromatic molecules at the oil-water interface: A molecular dynamics simulation study. *The Journal of Physical Chemistry B* 2014, 118 (4), 1040-1051.

(18) Jian, C.; Tang, T.; Bhattacharjee, S. Probing the effect of side-chain length on the aggregation of a model asphaltene using molecular dynamics simulations. *Energy Fuels* 2013, 27 (4), 2057-2067.

(19) Joonaki, E.; Buckman, J.; Burgass, R.; Tohidi, B. Water versus asphaltenes; Liquid-liquid and solid-liquid molecular interaction unravel the mechanisms behind an improved oil recovery methodology. *Sci. Rep.* 2019, 9, 11369.

(20) Wang, J.; Van Der Tuuk Opedal, N.; Lu, Q.; Xu, Z.; Zeng, H.; Sjöblom, J. Probing molecular interactions of an asphaltene model compound in organic solvents using a surface forces apparatus (SFA). *Energy Fuels* 2012, 26, 2591-2599.

(21) Wang, J.; Lu, Q.; Harbottle, D.; Sjöblom, J.; Xu, Z.; Zeng, H. Molecular interactions of a polyaromatic surfactant C5Pe in acqueous solutions studied by a surface forces apparatus. *J. Phys. Chem. B* 2012, 116, 11187-11196.

(22) Simon, S.; Jestin, J.; Palermo, T.; Barré, L. Relation between solution and interfacial properties of asphaltene aggregates. *Energy Fuels* 2009, 23 (1), 306-313.

(23) Eyssautier, J.; Levitz, P.; Espinat, D.; Jestin, J.; Gummel, J.; Grillo, I.; Barré, L. Insight into asphaltene nanoaggregate structure inferred by small angle neutron and X-ray scattering. *The Journal of Physical Chemistry B* 2011, 115 (21), 6827-6837.

(24) Mullins, O. C. The modified Yen model. *Energy Fuels* 2010, 24 (4), 2179-2207.

(25) de Boer, R. B.; Leerlooyer, K.; Eigner, M. R. P.; van Bergen, A. R. D. Screening of crude oils for asphalt precipitation: Theory, practice, and the selection of inhibitors. SPE Production & Facilities 1995, 55-61.

(26) Spiecker, P. M.; Gawrys, K. L.; Kilpatrick, P. K. Aggregation and solubility behavior of asphaltenes and their subfractions. *Journal of Colloid and Interface Science* 2003, 267 (1), 178-193.

(27) Spiecker, P. M.; Gawrys, K. L.; Trail, C. B.; Kilpatrick, P. K. Effects of petroleum resins on asphaltene aggregation and water-in-oil emulsion formation. *Colloids and Surfaces A: Physicochemical and Engineering Aspects* 2003, 220 (1-3), 9-27.

(28) Cardoso, F. M. R.; Carrier, H.; Daridon, J. L.; Pauly, J.; Rosa, P. T. V. CO2 and temperature effects on the asphaltene phase envelope as determined by a quartz crystal resonator. *Energy Fuels* 2014, 28 (11), 6780-6787.

(29) Fenistein, D.; Barré, L.; Frot, D. From aggregation to flocculation of asphaltenes, a structural description by radiation scattering techniques. *Oil & Gas Science and Technology* 2000, 55 (1), 123-128.

(30) Hoepfner, M. P.; Limsakoune V.; Chuenmeechao V.; Maqbool T.; Fogler H. S. A fundamental study of asphaltene deposition. *Energy Fuels* 2013, 27, 725-735.

(31) Goual, L.; Sedghi, M.; Wang, X.; Zhu, X. Asphaltene aggregation and impact of alkylphenols. *Langmuir* 2014, 30, 5394-5403.

(32) Firoozinia, H.; Abad, K. F. H.; Varamesh, A. A comprehensive experimental evaluation of asphaltene dispersants for injection under reservoir conditions. *Pet. Sci.* 2016, 13, 280-291.

(33) Marcano, F.; Moura, L. G. M.; Cardoso, F. M. R.; Rosa, P. V. T. Evaluation of the chemical additive effect on asphaltene aggregation in dead oils : A comparative study betwen ultraviolet-visible and near-infrared-laser light scattering techniques. *Energy Fuels* 2015, 29, 2813-2822.

(34) León, O.; Contreras, E.; Rogel, E.; Dambakli, G.; Acevedo, S.; Carbognani, L.; Espidel, J. Adsorption of native resins on asphaltene particles : A correlation between adsorption and activity. *Langmuir* 2002 18, 5106-5112.

(35) Higaki, Y.; Hatae, K.; Ishikawa, T.; Takanohashi, T.; Hayashi, J.-I.; Takahara, A. Adsorption and desorption behavior of asphaltene on polymer-brush-immobilized surfaces. *ACS Appl. Mater. Interfaces* 2014, 6, 20385-20389.

(36) Labrador, H.; Fernández, Y.; Tovar, J.; Muñoz, R.; Pereira, J. C. Ellipsometry study of the adsorption of asphaltene films on a glass surface. *Energy Fuels* 2007, 21, 1226-1230.

(37) Ekholm, P.; Blomberg, E.; Claesson, P.; Auflem, I. H.; Sjöblom, J.; Kornfeldt, A. A quartz crystal microbalance study of the adsorption of asphaltenes and resins onto a hydrophilic surface. *J. Colloid Interface Sci.* 2002, 247 (2), 342-350.

(38) Daridon, J. L.; Cassiède, M.; Nasri, D.; Pauly, J.; Carrier, H. Probing asphaltene flocculation by a quartz crystal resonator. *Energy Fuels* 2013, 27, 4639−4647.

(39) Tavakkoli, M.; Panuganti, S. R.; Vargas, F. M.; Taghikhani, V.; Pishvaei, M. R.; Chapman, W. G. Asphaltene deposition in different depositing environments : Part 1. Model oil. *Energy Fuels* 2014, 28, 1617-1628.

(40) Tavakkoli, M.; Panuganti, S. R.; Vargas, F. M.; Taghikhani, V.; Pishvaei, M. R.; Chapman, W. G. Asphaltene deposition in different depositing environments : Part 2. Real oil. *Energy Fuels* 2014, 28, 3594-3603.

(41) Joonaki, E.; Burgass, R.; Hassanpouryouzband, A.; Tohidi, B. Comparison of experimental techniques for evaluation of chemistries against asphaltene aggregation and deposition : new application of high-pressure and high-temperature quartz crystal microbalance. *Energy Fuels* 2018, 32, 2712-2721.

(42) Campen, S.; Moorhouse, S. J.; Wong, J. S. S. Mechanism of an asphaltene inhibitor in different depositing environments : Influence of colloid stability. *J. Pet. Sci. Eng.* 2020, 184, 10652.

(43) Campen, S.; Di Mare, L.; Smith, B.; Wong, J. S. S. Determining the kinetics of asphaltene adsorption from toluene: A new reaction-diffusion model. *Energy Fuels* 2017, 31, 9101-9116.

(44) Campen, S.; Smith, B; Wong, J. Deposition of asphaltene from destabilized dispersions in heptane-toluene. *Energy Fuels* 2018, 32, 9159-9171.

(45) Campen, S. M.; Moorhouse, S. J.; Wong, S. S. Effect of aging on the removal of asphaltene deposits with aromatic solvent. *Langmuir* 2019, 35, 11995-12008.

(46) Saidoun, M.; Palermo, T.; Passade-Boupat, N.; Gingras, J. P.; Carrier, H.; Daridon, J. L. Revisiting asphaltenes instability predictions by probing destabilization using a fully immersed quartz crystal resonator. *Fuel* 2019, 251, 523-533.

(47) Acevedo, N.; Moulian, R.; Chacón-Patiño, M. L.; Mejia, A.; Radji, S.; Daridon, J. L.; Barrère-Mangote, C.; Giusti, P.; Rodgers, R. P.; Piscitelli, V.; Castillo, J.; Carrier, H.; Bouyssiere, B. Understanding asphaltene fraction behavior through combined quartz crystal resonator sensor, FT-ICR MS, GPC ICP HR-MS, and AFM characterization. Part I: Extrography fractionations. *Energy Fuels* 2020, 34, 13903-13915.

(48) Daridon, J. L.; Carrier, H. Measurement of phase changes in live crude oil using an acoustic wave sensor: Asphaltene instability envelope. *Energy Fuels* 2017, 31, 9255-9267.

(49) Daridon, J. L.; Orlandi, E.; Carrier, H. Measurement of bubble point pressure in crude oils using an acoustic wave sensor. *Fluid Phase Equilibria* 2016, 427, 152−160.

(50) Daridon, J. L.; Lin, C. W.; Carrier, H.; Pauly, J.; Fleming, F. P. Combined investigations of fluid phase equilibria in complex CO_2-crude oil systems under high pressure. *J. Chem. Eng. Data* 2020, 65, 3357-3372.

(51) Cassiède, M.; Daridon, J. L.; Paillol, J. H.; Pauly, J. Electrical behavior of a quartz crystal resonator immersed in a pressurized fluid (gas or liquid). *J. Appl. Phys.* 2011, 109, 074501.

(52) Goual, L.; Horváth-Szabó, G.; Masliyah, J. H.; Xu, Z. Adsorption of bituminous components at oil/water interfaces investigated by quartz crystal microbalance: Implications to the stability of water-in-oil emulsions. *Langmuir* 2005, 21, 8278-8289.

(53) Passade-Boupat, N.; Gingras, J. P.; Desplobins, C.; Zhou, H. Could the asphaltene solubility class index be used as the "Wax Appearance Temperature" of asphaltenes? Illustration through the study of the polydispersity of PetroPhase 2017 asphaltenes. *Energy Fuels* 2018, 32 (3), 2760-2768.

(54) Rüger, C. P.; Grimmer, C.; Sklorz, M.; Neumann, A.; Streibel, T.; Zimmermann, R. Combination of different thermal analysis methods coupled to mass spectrometry for the analysis of asphaltenes and their parent crude oils: Comprehensive characterization of the molecular pyrolisis pattern. *Energy Fuels* 2018, 32, 2699-2711.

(55) Giraldo-Dávila, D.; Chacón-Patiño, M. L.; McKenna, A. M.; Blanco-Tirado, C.; Combariza, M. Y. Correlations between molecular composition and adsorption, aggregation, and emulsifying behaviors of PetroPhase 2017 asphaltenes and their thin-layer chromatography fractions. *Energy Fuels* 2018, 32, 2769-2780.

(56) Lin, Y. J.; Cao, T.; Chacón-Patiño, M. L.; Rowland, S. M.; Rodgers, R. P.; Yen, A.; Biswal, S. L. Microfluidic study of the deposition dynamics of asphaltene subfractions enriched with island and archipelago motifs. *Energy Fuels* 2019, 33, 1882-1891.

(57) Moulian, R.; Sama, S. G.; Garnier, C.; Mounicou, S.; Enrico, M.; Jaurand, X.; Lobinski, R.; Giusti, P.; Bouyssiere, B.; Barrère-Mangote, C. Speciation of metals in asphaltenes by high-performance thin-layer chromatography and laser ablation inductively coupled plasma-mass spectrometry. *Energy Fuels* 2019, 33, 6060-6068.

(58) Putman, J. C.; Moulian, R.; Barrère-Mangote, C.; Rodgers, R. P.; Bouyssiere, B.; Giusti, P.; Marshall, A. G. Probing aggregation tendencies in asphaltenes by gel permeation chromatography. Part 1: Online inductively coupled plasma mass spectrometry and offline Fourier transform ion cyclotron resonance mass spectrometry. *Energy Fuels* 2020, 34, 8308-8315.

(59) Putman, J. C.; Moulian, R.; Smith, D. F.; Weisbrod, C. R.; Chacón-Patiño, M. L.; Corilo, Y. E.; Blakney, G. T.; Rumancik, L. E.; Barrère-Mangote, C.; Rodgers, R. P.; Giusti, P.; Marshall, A. G.; Bouyssière, B. Probing aggregation tendencies in asphaltenes by gel permeation chromatography. Part 2: Online detection by Fourier transform ion cyclotron resonance mass spectrometry and inductively coupled plasma mass spectrometry. *Energy Fuels* 2020, 34, 10915-10925.

(60) Chacón-Patiño, M. L.; Vesga-Martínez, S. J.; Blanco-Tirado, C.; Orrego-Ruiz, J. A.; Gómez-Escudero, A.; Combariza, M. Y. Exploring occluded compounds and their interactions with asphaltene networks using high-resolution mass spectrometry. *Energy Fuels* 2016, 30, 4550-4561.

(61) Cassiède, M.; Daridon, J. L.; Paillol, J. H.; Pauly, J. Characterization of the behaviour of a quartz crystal resonator fully immersed in a Newtonian liquid by impedance analysis. *Sens. Actuators, A* 2011, 167 (2), 317−326.

(62) Verruto, V. J.; Kilpatrick, P. K. Water-in-model oil emulsions studied by small-angle neutron scattering: Interfacial film thickness and composition. *Langmuir* 2008, 24 (22), 12807-12822.

(63) Jestin, J.; Simon, S.; Zupancic, L.; Barré, L. A small angle neutron scattering study of the adsorbed asphaltene layer in water-in-hydrocarbon emulsions: Structural description related to stability. *Langmuir* 2007, 23 (21), 10471-10478.

(64) Knudsen, K. D.; Simon, S.; Geue, T.; Cooper, J. F. K.; Sjöblom, J. Interactions between asphaltenes and a model demulsifier in bulk and at an interface studied by small-angle neutron scattering (SANS) and neutron reflectometry. *Energy Fuels* 2020, 34 (6), 6768-6779.

(65) Iloukhani, H.; Rezaei-Sameti, M.; Basiri-Parsa, J. Excess molar volumes and dynamic viscosities for binary mixtures of toluene + n-alkanes (C5-C10) at T = 298.15 K – Comparison with Prigogine-Flory-Patterson theory. *J. Chem. Thermodyn.* 2006, 38 (8), 975-982.

(66) Baylaucq, A.; Boned, C.; Canet, X.; Zéberg-Mikkelsen, C. K. High-pressure (up to 140 MPa) dynamic viscosity of the methane and toluene system: Measurements and comparative study of some representative models. *Int. J. Thermophys.* 2003, 24 (3), 621-638.

(67) Legret, D.; Richon, D.; Renon, H. Vapor-liquid equilibria of methane-benzene, methane-methylbenzene (toluene), methane-1,3-dimethylbenzene (m-xylene), and methane-1,3,5-trimethylbenzene (mesitylene) at 313.2 K up to the critical point. *J. Chem. Eng. Data* 1982, 27, 165-169.

(68) Lin, Y. N.; Hwang, S. C.; Kobayashi, R. Vapor-liquid equilibrium of the methane-toluene system at low temperatures. *J. Chem. Eng. Data* 1978, 23 (3), 231-234.

(69) Hugues, T. J.; Kandil, M. E.; Graham, B. F.; Marsh, K. N.; Huang, S. H.; May, E. F. Phase equilibrium measurements of (methane + benzene) and (methane + methylbenzene) at temperatures from (188 to 348) K and pressures to 13 MPa. *J. Chem. Thermodynamics* 2015, 85, 141-147.

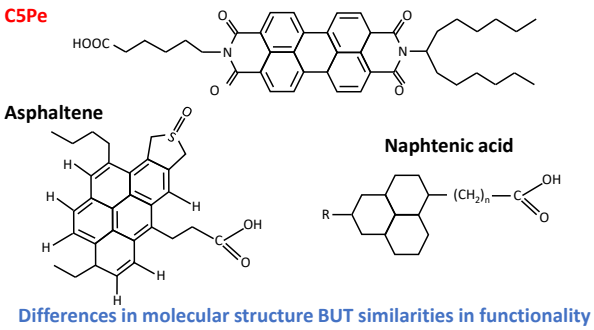
C5Pe
HOOC
N
O
Asphaltene
Naphtenic acid
R
OH
Differences in molecular structure BUT similarities in functionality

TOC graphic